Available online at www.sciencedirect.com

ScienceDirect

Procedia Engineering 102 (2015) 1006 – 1015

Procedia Engineering

www.elsevier.com/locate/procedia

The 7th World Congress on Particle Technology (WCPT7)

Application of Temperature and Pressure Signals for Early Detection of Defluidization Conditions

Jaber Shabanian, Pierre Sauriol, Abdelmajid Rakib, Jamal Chaouki*

Department of Chemical Engineering, Ecole Polytechnique de Montreal, Montreal, Quebec, Canada

Abstract

This work shows that simultaneous measurements of temperature and pressure signals for a bubbling gas-solid fluidized bed can be considered as a simple and effective early detection technique of defluidization conditions. The modification of the hydrodynamics of the bed due to the presence of interparticle forces (IPFs) was primarily investigated using different measurement techniques (i.e., pressure transducers, optical fiber probe, and Radioactive Particle Tracking). Different levels of IPFs were attained in the bed with the help of a polymer coating approach at near-ambient temperature (30–40°C) in a 15 cm ID fluidized bed. Experimental results showed that by increasing the degree of IPFs in the bed, larger bubbles were noted at gas velocities well above the minimum fluidization velocity, the emulsion phase voidage increased, and the mean value of the in-bed differential bed pressure drop and the axial solids mixing decreased. The high temperature defluidization tests (800–1000°C) as the second part the experimental campaign were conducted in a 20 cm ID fluidized bed reactor. It was found that the temperature difference between the bottommost thermocouple (located 5 cm above the distributor) and the others located in the dense bed was continuously increasing when the bed was approaching defluidization. Simultaneously, the mean value of the differential pressure signals was successively decreasing from its regular value under normal conditions. A combination of these two conditions was considered as the monitoring method for the early detection of defluidization. It was found that this approach was effectively capable of predicting the onset of defluidization minutes to hours before complete defluidization, allowing time to apply counteracting strategies. Experimental results of the first part of the work clearly demonstrated why the simple integrated approach discovered in the second part of the study can be efficiently used for timely recognition of defluidization conditions.

Selection and peer-review under responsibility of Chinese Society of Particuology, Institute of Process Engineering, Chinese Academy of Sciences (CAS)

* Corresponding author. Tel.: +1-514-340-4711 Ext. 4034; fax: +1-514-340-4159.
E-mail address: jamal.chaouki@polymtl.ca

Selection and peer-review under responsibility of Chinese Society of Particuology, Institute of Process Engineering, Chinese Academy of Sciences (CAS)
doi:10.1016/j.proeng.2015.01.223

Keywords: Defluidization detection; Gas-solid fluidized bed; Temperature measurements; Differential pressure fluctuation measurements

1. Introduction

With the rarefaction of conventional energy feedstocks and the efforts to reduce greenhouse gas emissions, it is expected that high temperature fluidized beds are going to be adapted to process new or unconventional energy feedstocks (biomass, various waste materials, low grade coal) or blends (co-firing with conventional fuels). However, these new feedstocks may have high alkali/alkali earth content, which are known to form low melting eutectics at elevated temperatures. The presence of these eutectics inside the bed can induce the formation of agglomerates (bed material and ash), which when accumulating may eventually result in the defluidization of the bed and the unscheduled shut down of the plant. It is thus important to prevent or delay the onset of defluidization incidents. There are a number of counteracting strategies for delaying the onset of defluidization (e.g., lowering the temperature, increasing the superficial gas velocity, high velocity jets, injection of solid additives, semicontinuous replacement of bed material). As these strategies can incur a temporary offset of the fluidized bed performance (e.g., lower efficiency, residue production or added material cost), they should be used sparingly upon opportune detection of the onset of defluidization.

Siegell [1] described the defluidization phenomenon as a direct consequence of the stickiness of bed material. Different methods have been proposed to determine if the bed behavior is moving toward a defluidization state or not. The simplicity, reliability, and robustness of the identification approach as well as its capability for early detection are the most important criteria. Siegell [2] and Tardos et al. [3, 4] were the first to introduce that defluidization is accompanied by a rapid decrease in the total bed pressure drop because most of the fluidizing gas flows through large channels when defluidization occurs. The main drawback with this method is late detection, i.e., when the bed is already partially defluidized. Several other measurement tools, such as capacitance and optical fiber probes, heat transfer probes, and electrodes for measuring triboelectric current [5], which have small measurement volumes, are only useful for determining whether or not small regions are defluidized [6]. These approaches would require many measurement points for a large-scale fluidized bed. Furthermore, these intricate measurement techniques, which are frequently used in academia, have not seen widespread use in industrial applications. On the other hand, temperature and pressure measurements are the only routine measurements available for industrial fluidized beds [7].

In comparison to the other measurement techniques considered, pressure probes have a much larger detection volume (in the order of some tens of centimeters) [8, 9]. Accordingly, they can provide more practical information with the least number of measurement points about the quality of the fluidization. Moreover, the measurement of pressure signals in a gas-solid fluidized bed is relatively easy to perform, nonintrusive, cost-effective and includes the impact of many phenomena happening in the bed, such as bubble formation, coalescence, eruption, movement and bed mass oscillations [10, 11]. Chirone et al. [12] had applied a relatively simple method, i.e., variance of pressure signals, for the early detection of defluidization. However, since the standard deviation/variance of pressure signals recorded from a gas-solid fluidized bed depends on fluctuations in the gas flow [13], this method is too sensitive to other process changes, leading to false alarms. Hence, this is not considered as a reliable approach for the advanced detection of defluidization in an industrial process [14]. Van Ommen et al. [15] developed an attractor comparison approach that is based on the measurement of pressure signals in the bed for the early warning of defluidization. Although, this technique demonstrated a good performance in the timely recognition of defluidization on both laboratory and pilot scale fluidized beds, it requires many mathematical manipulations and suffers from occasional false alarms, especially when an operational strategy is applied to the system to prevent complete defluidization [14]. This could be principally due to the sole dependence of the detection method on the pressure measurements. The temperature measurements can provide indirect information about the fluidization characteristics, but require considerable insight into the corresponding process to result in a correct interpretation [7].

It can be inferred that the sole application of either temperature or pressure signals alone cannot yield a simple, robust and efficient method for the early detection of defluidization, as the risk of false positives and false negatives has been observed, especially when applying operational changes to a system. The present work will attempt to propose a robust criterion for the early detection of the defluidization phenomenon using temperature and pressure

signal data, specifically targeted at the conditions that may exist in a bubbling fluidized bed combustor using coarse sand particles as bed material.

Before attempting to implement the technique at high temperature conditions, the first part of the work focused on the study of bubbling fluidized beds of model particles with varying degrees of IPFs at near-ambient conditions (e.g., 30–40^{o}C). In particular, the polymer coating approach [16, 17] was used to introduce different levels of IPFs into a gas-solid fluidized bed. Different measurement techniques (i.e., pressure transducers, optical fiber probe, and Radioactive Particle Tracking (RPT)) were applied with this approach to both locally and globally highlight the effect of IPFs on the fluidization behavior of the bed. The findings were then extrapolated to high temperature conditions.

Nomenclature

Acronyms

CSB30	Coated Sugar Beads at 30^{o}C
CSB40	Coated Sugar Beads at 40^{o}C
IPFs	Interparticle Forces
RPT	Radioactive Particle Tracking
SB20	Fresh Sugar Beads at 20^{o}C

Symbols

D	Column diameter (m)
d_p	Mean particle size (μm)
h	Bed height (m)
U_c	Transition velocity from bubbling to turbulent regime (m/s)
U_g	Gas velocity (m/s)
U_{mf}	Minimum fluidization velocity (m/s)
$U_{mf,\ SB20}$	Minimum fluidization velocity for SB20 (m/s)
$U_{mf,\ No\ IPFs}$	Minimum fluidization velocity for a bed without IPFs (m/s)
$U_{c,\ No\ IPFs}$	Transition velocity from bubbling to turbulent regime for a bed without IPFs (m/s)
ε_e	Emulsion phase voidage (m/s)
ρ_p	Particle density (kg/m^3)

2. Experimental

2.1. Investigation of the effect of IPFs on the hydrodynamics of the bed

The first experimental step was to study the influence of IPFs on the fluidization behavior of the bed. A polymer coating approach [16, 17] was employed to enhance and adjust the level of cohesive IPFs in a gas-solid fluidized bed. The experimental work initially required the production of base particles uniformly coated with a thin polymer film of PMMA/PEA (Poly Methyl MethAcrylate/Poly Ethyl Acrylate). It was achieved through an atomization process in a spheronizer machine. A 450-700 μm cut of spherical sugar beads (d_p=580 μm, ρ_p=1556 kg/m^3), which belong to Geldart group B particles at ambient conditions, was used as the inert base particles. The thickness of the coating layer was approximately 5.0 μm. Details of the coating procedure and its operating conditions have been previously outlined [16, 18-20].

Following the coating process, the coated particles and the fresh sugar beads were separately used in a cold gas-solid fluidized bed operating under atmospheric pressure with a 15.2 cm internal diameter. Dried and filtered air was used as the fluidizing gas and introduced through a perforated distributor plate (consisting of 157 holes 1 mm in diameter) into the column. In order to investigate the effect of IPFs on the fluidization behavior of the bed,

experiments with fresh sugar beads as the base system without IPFs were conducted at 20°C while experiments with the coated sugar beads were carried out at 30°C and 40°C. For the sake of simplicity these systems are referred to by their corresponding operating temperatures, SB20, CSB30, and CSB40, which stand for fresh sugar beads at 20°C, and coated sugar beads at 30°C and 40°C, respectively. At each temperature tested, different superficial gas velocities were used (up to 1.3 m/s), covering both bubbling and turbulent fluidization regimes.

The fluidization tests were carried out for the purpose of hydrodynamic study employing different measurement techniques, i.e., pressure transducers, optical fiber probe, and RPT. Measurements of the pressure signals were taken by the application of four individual pressure transducers and carried out by measuring the bed pressure drop (0.95–300 cm above the distributor), and registering the gauge and differential pressure signals in the dense bed (17.5 cm and 10–25 cm above the distributor, respectively) and the gauge pressure signals in the windbox. A reflective type solids concentration optical fiber probe, located at the center of the column and 20 cm in height above the distributor, was also used to measure the instantaneous local bed voidage. For the fluidization tests with these two measurement techniques 4.0 kg of material were introduced into the bed, which resulted in a static bed height of approximately 26 cm (h/D≈1.7) at ambient conditions. Measurements of the pressure signals and the instantaneous local bed voidage were simultaneously carried out for a period of four minutes with a sampling frequency of 400 Hz at each superficial gas velocity and temperature tested. The calibration curve developed by Cui et al. [21] was employed to calibrate the optical fiber probe. Hydrodynamic tests with the application of the RPT technique were carried out for SB20 and CSB40 at two different superficial gas velocities (0.30 and 0.50 m/s) in the bubbling regime while 3 kg of material were introduced into the column. A sampling time of 10 ms was used in these tests and each experiment lasted 4 hours. More detail about the RPT experiment can be found elsewhere [20].

2.2. High temperature defluidization tests

All experiments related to high temperature defluidization were conducted in an atmospheric pressure pilot scale fluidized bed reactor with a 20 cm internal diameter. Air was used as the fluidizing gas and injected through a bubble cap distributor plate (with 9 caps each having 4 holes on its perimeter) into the column. For this investigation, the bed consisted of about 30 kg of coarse silica sand (d_p=830 μm, ρ_p=2650 kg/m^3). Thermocouples were positioned along the length of the fluidized bed with the bottommost one located only 5 cm above the distributor. Using these thermocouples the uniformity of the temperature profile along the bed could be monitored. Also, two differential pressure transducers recorded pressure signals from the bed. One was used to approximately measure the total pressure drop across the bed (5–130 cm above the distributor). The other one recorded the differential pressure drop from the central part of the dense bed (15–45 cm above the distributor). Throughout the runs, the superficial velocity of the air entering the fluidized bed was kept constant at 1 m/s. The bed defluidization was induced by combusting coal coated with alkali/alkali-earth containing materials. The bed was successively operated for periods of 1 hour at a time at 800, 900 and 1000°C using the same solid fuel. Propane gas was used between each temperature point to increase the bed temperature. In cases where the alkali content was high enough, the bed became defluidized either in the heat-up pass with propane or during the solid fuel combustion. Pressure and temperature measurements were simultaneously conducted during the test with the sampling frequencies of 400 and 1 Hz, respectively.

3. Results and discussion

3.1. Effect of IPFs on the hydrodynamics of the bed

Van der Schaaf et al. [10] proposed a frequency-domain-based approach to be applied on the pressure signals recorded in the dense bed to estimate the bubble length scale in the bed. In this method, the registered in-bed gauge/absolute pressure signals are decomposed into their coherent (≈ COP) and incoherent (≈ IOP) power spectral densities by a frequency-domain-based coherence function in relation to identical types of pressure signals recorded in the windbox. The IOP component represents the power spectral density of pressure signals arising from the local bubble passage. Therefore, according to Parseval's theorem, the integral of IOP in the frequency domain yields the

variance of the IOP components of pressure signals in the time domain. This is proportional to the characteristic length scale of the bubble, which is an approximation of the exact volume-based average bubble size [22].

Fig. 1 illustrates the bubble sizes estimated by the IOP method as a function of gas velocity U_g for systems differing in the level of IPFs. An approximately linear increase in the estimated bubble size with the gas velocity can be found in Fig. 1 for all systems studied. The slope in the bubble size versus gas velocity increased with IPFs while a bed with a higher level of IPFs contained slightly smaller bubbles at low gas velocities. It covered the range of gas velocities approximately below $3U_{mf,\ SB20}$, where $U_{mf,\ SB20}$ is the minimum fluidization for SB20 (0.18 m/s). This behavior resulted in a trend inversion at moderate gas velocity. The CSB40, a system with the highest level of IPFs, contained the largest bubbles at gas velocities above 0.65 m/s. It should be noted that depending on the level of IPFs and physical properties of the fluidizing gas and particles, the inversion trend can happen at different ratios of $U_g/U_{mf,\ No\ IPFs}$. It can be also found that by increasing the level of IPFs, the transition velocity from bubbling to turbulent regime U_c, where large bubbles are replaced by smaller and transient voids [23], increased toward higher gas velocities.

The method of the minimum probability of local bed voidage [24] was employed to distinguish the emulsion phase from the bubble phase from the instantaneous local bed voidage signals measured by the optical fiber probe. Subsequently, the time-averaged voidage of the emulsion phase was calculated at each operating condition and plotted in Fig. 2. It shows that the emulsion phase voidage ε_e progressively increased with the level of IPFs for the gas velocities below 0.7 m/s, where all systems were operating in the bubbling regime from the meso-scale point of view [20]. This implies that the capacity of the emulsion phase for holding the fluidizing gas inside its structure increased with the degree of IPFs in the gas-solid fluidized bed. The presence of a plateau-like region for the variation of the emulsion phase voidage with the gas velocity confirms the resistance shown by the emulsion phase against the complete breakdown of its continuous structure. The complete breakdown of the emulsion phase, which can be translated into the disappearance of the stable two-phase flow structure with a clear boundary between the bubble and emulsion phases, is necessary for the local flow regime transition from bubbling to turbulent [20, 25]. It can be observed from Fig. 2 that this stable level occurred at lower gas velocities and covered a narrower velocity range for systems with a lower amount of IPFs. This indicates that IPFs can stabilize the emulsion phase from any changes that can be imposed on its structure; hence, the formation of the stalactite of particles on the bubble's roof, which is responsible for the bubble splitting [26], decreases with IPFs. Accordingly, the rate of bubble splitting decreases by increasing the level of IPFs in the bed. This results in a slight increase in the growth rate of bubbles with the gas velocity and also an increase in U_c for a system with a higher degree of IPFs (refer to Fig. 1).

By considering Fig. 1 in conjunction with Fig. 2, it can be found that ε_e was perceptibly smaller for SB20 in comparison with CSB30 and CSB40 for gas velocities below 0.5 m/s. In this range of low gas velocities, the emulsion phase was the main constituent of the bed while slightly smaller bubbles were noted for a bed with a higher degree of IPFs. These hydrodynamic modifications suggest that if differential pressure drop signals are measured for the central (well stabilized) part of the dense bed while it is operating at low gas velocities, the average in-bed differ-

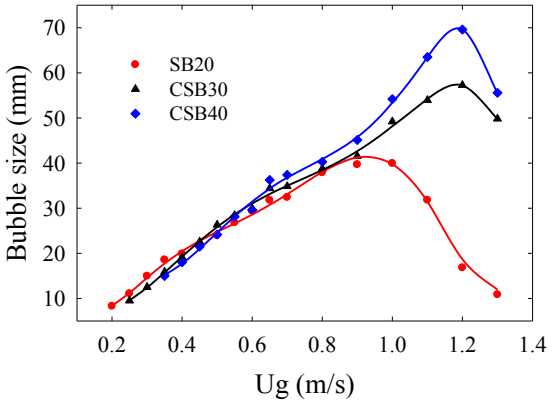

Fig 1. Influence of IPFs on the bubble size estimated by IOP method.

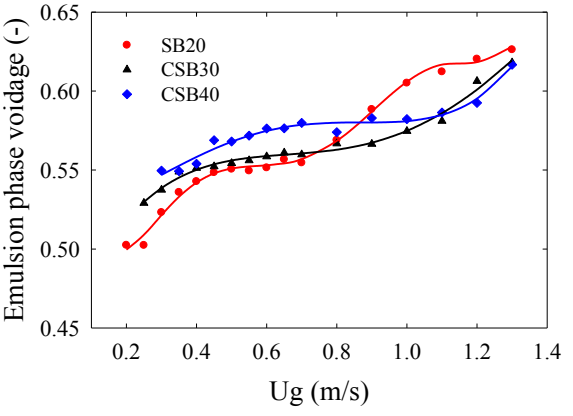

Fig 2. Influence of IPFs on the emulsion phase voidage.

-ential pressure drop decreases with IPFs since the permeability of the emulsion phase can be greatly enhanced by IPFs. At moderate and high gas velocities (0.5-0.9 m/s), where all beds were operating in the bubbling regime (refer to Fig. 1), the emulsion phase remained more diluted for a bed with a higher level of IPFs while it contained larger bubbles. Thus, an increase in the level of IPFs under such operating conditions offers a higher reduction in the mean value of the in-bed differential pressure drop measurement. In a consistent manner, it can be found in Fig. 3 that the average in-bed differential pressure drop measured by a corresponding pressure sensor for the stabilized section of the bubbling dense bed was lower for beds with stronger IPFs, while the total bed pressure drops of systems with different levels of IPFs were closely identical to each other. By a progressive increase in the level of IPFs, it is expected that the mean value of the in-bed differential pressure drop further decreases and even demonstrates a sudden decrease once the bed is at the final defluidization state. This could be accompanied by a rapid decrease in the total pressure drop of the bed. The presence of large channels that form throughout the bed by the fluidizing gas under that operating condition is primarily responsible for this behavior. At gas velocities higher than 0.9 m/s, complex trends for the in-bed differential pressure drops of systems with different levels of IPFs can be noted since SB20 transferred into the turbulent regime first and the amount of bed material decreased due to entrainment. Accordingly, the reduction in the mean value of the in-bed differential pressure drop due to the increase in the level of IPFs is credible for the span of gas velocities below the transition velocity from bubbling to turbulent regime for a bed without IPFs ($U_{c,No\ IPFs}$).

In the bubbling fluidized beds, the passage of bubbles plays the principle role in the formation and evolution of the flow structure of the bed as well as the movements of particles, more generally solids mixing. Also, the heat and mass transfer rates are in close relation with the solids motion in the bed [27]. Particles are carried by the rising bubbles to the splash zone. To compensate this upward movement, a downward flow of particles along the annulus exists in the bed. Stein et al. [28] defined the cycle frequency, as the average frequency of a tracer particle to complete a cycle that starts in the bottom 30% of the dense bed height, takes it to the top 30% and returns it back to the bottom, as a characteristic of the axial solids mixing in the bed.

The time-position trajectory of particles obtained from the RPT experiments was used to calculate the cycle frequency under different operating conditions. Fig. 4 illustrates the results of this evaluation. It shows that the cycle frequency increased by the gas velocity for both SB20 and CSB40 in the bubbling regime. This can be attributed to the increase in the turbulent activity of bubbles in the bed; hence, particles can be more frequently picked up by the rising bubbles, move with them toward the splash zone and return back to the bottom zone of the bed with a higher rate to maintain the continuity. The cycle frequency decreased by increasing the level of IPFs. It reveals that axial movement of particles occurred with a higher degree of difficulty in a bed with stronger IPFs. In general, the high degree of solids mixing is responsible for the uniformity of temperature and composition in the fluidized bed [27]. Therefore, this result suggests that increasing the level of IPFs decreases the axial solids mixing in the bubbling flui-

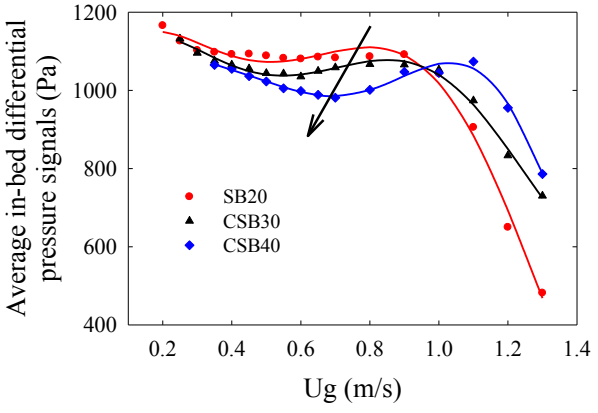

Fig 3. Influence of IPFs on the average in-bed differential pressure signals.

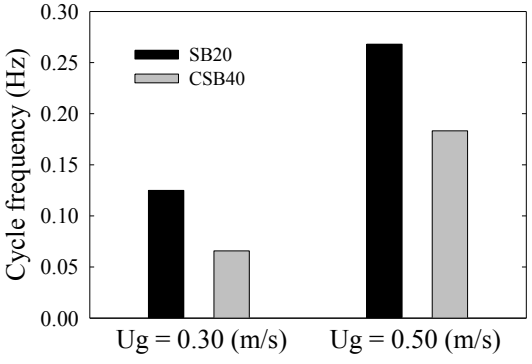

Fig 4. Influence of IPFs on the cycle frequency.

-dized bed. This can in turn reduce the temperature uniformity (increase the temperature gradient) along the bed height.

The experimental results obtained from the first part of this study provided two promising findings in relation to the early detection of defluidization for a bubbling gas-solid fluidized bed. It can be inferred that by moving toward the defluidization condition the average in-bed differential bed pressure drop decreases whereas the axial temperature gradient increases. The simultaneousness of the two observations as the bubbling fluidized bed approaches defluidization lends credence to the two independent measurement techniques that could be used to yield a robust defluidization early detection criterion. The second part of this study focuses on high temperature defluidization experiments to verify this hypothesis.

3.2. Early detection of defluidization conditions

Defluidization occurred in many high temperature experiments either during the solid fuel combustion or the subsequent heating step between the predefined operating temperatures (800, 900, and 1000^{o}C) by the in-bed combustion of propane. All high temperature defluidization experiments exhibited a qualitatively similar behavior. Hence, a typical example is provided here.

Figs. 5-7 show the temperature, total bed pressure drop, and in-bed differential pressure drop profiles as function of operating time for a fluidized bed that became defluidized during the experimental campaign. The bed was fluidizing well during the solid fuel combustion at 900^{o}C, which can be observed from the bed axial temperature profile. However, upon increasing the bed temperature, starting around the operating time 460 min, the readings of T4 (the bottommost thermocouple located only 5 cm above the distributor) began to deviate from those of other in-bed thermocouples. Simultaneously, a slight decrease in the in-bed differential pressure drop was observed. Nonetheless, no sensible change was noted for the total bed pressure drop. While not applying counteractive methods, these trends persisted until the complete defluidization of the bed some 40 minutes after the initial observation. Around the operating time 470 min, the difference between the readings of T4 and T6 (20 cm above the distributor) was about 15-20^{o}C while this difference was less than 8^{o}C under normal conditions. Also, a reduction of about 8% in the average in-bed differential pressure drop could be noted at the same time. In addition to the decrease in the quality of axial solids mixing when the bed is affected by the presence of IPFs, there could be also some small agglomerates being present in the lower section of the bed, hence, further deteriorating the solids mixing and resulting in a higher temperature gradient. It is worth mentioning that a variation of less than 3% was measured for the average in-bed differential pressure drop for the span of gas velocities and bed temperatures between 0.8–1.2 m/s and 800–1000^{o}C, respectively, when the bed was operating in the bubbling regime. This shows the relative independence of this parameter from variations in the gas velocity and operating temperature in the ranges tested. The decrease in the average in-bed differential pressure drop and increase in the temperature gradient clearly accelerated as the bed was further approaching the point of defluidization. The bed eventually became partially/completely defluidized around the operating time 500 min, where rapid decreases in the whole bed and in-bed differential pressure drops were noted, most likely due to the passage of fluidizing gas within the bed through channels. They were accompanied by a completely erratic behavior in the temperature profile in the bed, as the loss of fluidization (locally) results in a decrease in the heat transfer rate between the solid-gas and the thermocouple.

This experimental sample confirms that monitoring the whole bed pressure drop results in a very late detection of the defluidization condition. It also demonstrates that the simultaneous monitoring of the temperature profile with a special attention to the temperature difference between the bottommost level and higher levels in the dense bed and the in-bed differential pressure drop for the bed material considered can effectively identify the defluidization phenomenon much earlier than the final state. It also shows that both of these trends can concurrently take place when the level of IPFs is high enough to drive a bubbling bed of coarse silica sand toward the final defluidization point. Although this is a simple approach, its promising performance in the advanced recognition of defluidization allows appropriate measures to be taken to avoid a potential shutdown. According to this method, the operating time at which both of these trends are simultaneously noted for a bubbling gas solid fluidized bed (while the gas velocity remains relatively constant) can be considered as the starting point for applying counteracting measures against the defluidization phenomenon. Moreover, since the monitoring parameters of the method (temperature profile and the

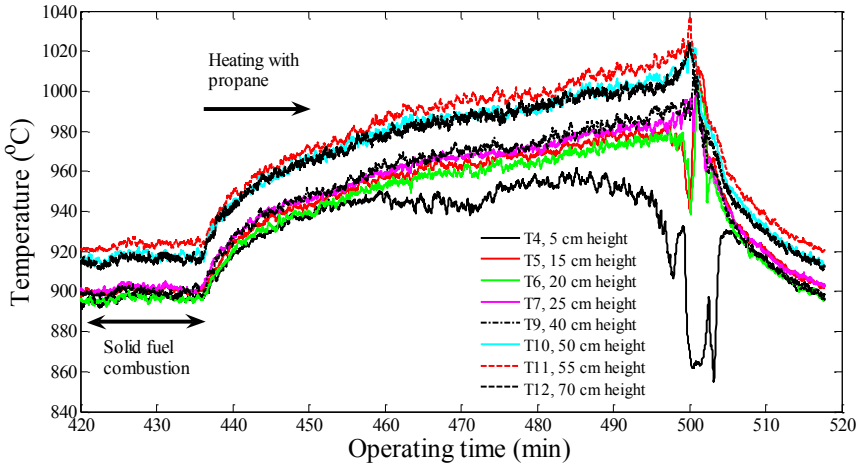

Fig 5. Typical temperature profile versus operating time for a fluidized bed approaching the defluidization condition.

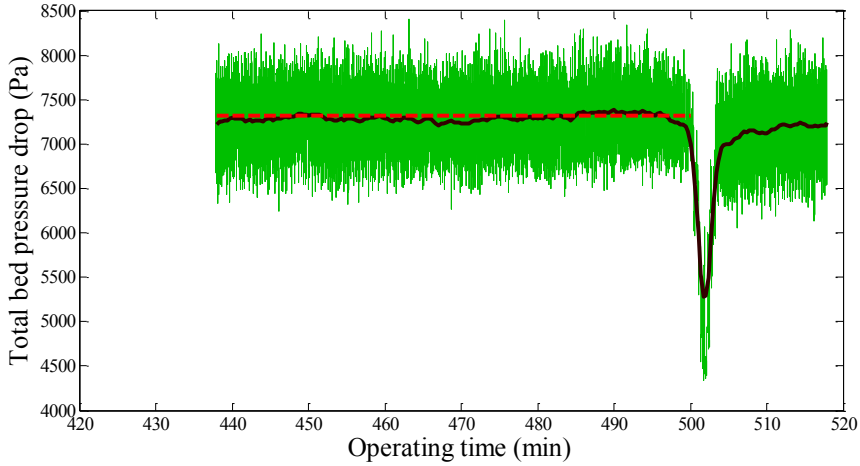

Fig 6. Typical bed pressure drop profile versus operating time for a fluidized bed approaching the defluidization condition.

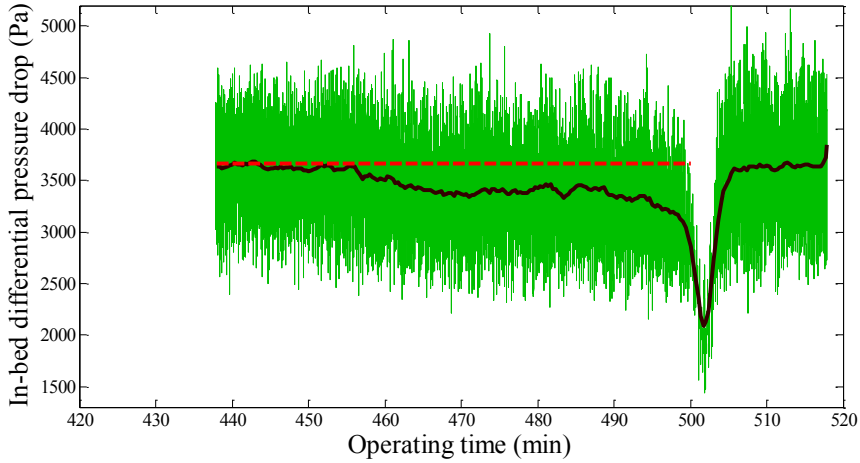

Fig 7. Typical in-bed differential pressure drop profile versus operating time for a fluidized bed approaching the defluidization condition.

average in-bed differential pressure drop) are relatively insensitive to variations of the gas velocity (in the bubbling regime) and operating temperature (800–1000°C, tested here), it can show a great robustness (in light of avoiding false alarms) in the early detection of defluidization.

It is worth mentioning that the defluidization sample provided here occurred during the combustion of propane inside the bed, which was fed through a horizontal tube, located some 20 cm above the distributor plate near the central axis of the bed. This was the case with most observed defluidization incidents and is explained by the fact that the reaction rates of propane and solid fuels differ significantly in the temperature range under investigation (<1 s for propane and ~1 min for coal). As a result, the combustion of propane and the ensuing heat release occurs in the vicinity of the propane injection point resulting in a higher temperature locally, which will have accelerated the formation of eutectics at the surface of bed materials in contact with this hot gas. Accordingly, the defluidization incident shown took place at an accelerated rate in comparison to that which would take place with solid fuels. In the case of solid fuels having high alkali content, defluidization can take place several hours after the early detection, allowing for a wider range of counteracting methods. As exhibited in Figs. 5-7, such a counteracting method could include an increase in superficial velocity combined with a reduction of the bed temperature to gain more time in case of rapid defluidization systems, such as a gas combusting system, to pace the implementation of more delicate corrective measures with potential system impacts, such as the replacement of the bed material, the injection of counteracting minerals, or the modification in fuel composition.

4. Conclusion

With the help of different experimental techniques, it was found that by increasing the level of IPFs in a bubbling gas-solid fluidized bed the hydrodynamics of the bed alters toward the presence of a more diluted emulsion phase, the formation of slightly smaller bubbles at gas velocities slightly higher than $U_{mf,\ No\ IPFs}$ and larger bubbles at high velocities of the bubbling regime as well as a reduction in the quality of axial solids mixing in the bed. These modifications suggest that the temperature gradient along the height of the bed increases and the average in-bed differential pressure drop decreases with IPFs.

With this phenomenological background, a simple and robust method is introduced for the early recognition of the defluidization condition for a bed of coarse particles operated in the bubbling regime. The method is based on simultaneous monitoring of temperature and pressure signals recorded for a bubbling gas-solid fluidized bed. According to this method, when a bubbling bed is approaching defluidization, the temperature gradient between readings of thermocouples located just above the distributor and those at higher levels of the bed increases over the operating time. At the same time, the mean value of an in-bed differential pressure drop demonstrates a continuous decrease over the shift toward defluidization. Although either of these two changes occurs in a bubbling fluidized bed that approaches defluidization, in order to make the detection method efficient and robust, a combination of these conditions should be satisfied simultaneously. Since the identification approach is taking advantage of the application of two measurement techniques that are common in industrial fluidized bed applications, it can be easily used in industrial applications. Moreover, the complete independence between temperature and pressure measurements, which are integrated in this method, reduces the chance of a false detection.

Acknowledgements

The authors would like to thank the Total American Service Inc. and the National Sciences and Engineering Research Council of Canada (NSERC) for their financial support of the present work.

References

[1] J.H. Siegell, Defluidization phenomena in fluidized bed of sticky particles at high temperature, The City University of New York, 1976.
[2] J.H. Siegell, High-temperature defluidization, Powder Technol. 38 (1984) 13–22.
[3] G. Tardos, D. Mazzone, R. Pfeffer, Destabilization of fluidized beds due to agglomeration part I: Theoretical model, Can. J. Chem. Eng. 63 (1985) 377–383.
[4] G. Tardos, D. Mazzone, R. Pfeffer, Destabilization of fluidized beds due to agglomeration part II: Experimental verification, Can. J. Chem.

Eng. 63 (1985) 384–389.
[5] C.L. Briens, L.A. Briens, E. Barthel, J.M. Le Blevec, A. Tedoldi, A. Margaritis, Detection of local fluidization characteristics using the V statistic, Powder Technol. 102 (1999) 95–103.
[6] J.R. van Ommen, R.-J. de Korte, C.M. van den Bleek, Rapid detection of defluidization using the standard deviation of pressure fluctuations, Chem. Eng. Process. 43 (2004) 1329–1335.
[7] J. Werther, Measurement techniques in fluidized beds, Powder Technol. 102 (1999) 15–36.
[8] J.F. Davidson, The two-phase theory of fluidization: successes and opportunities, AIChE Symp. Ser. 281 (1991) 1–12.
[9] J. Ruud van Ommen, J. van der Schaaf, J.C. Schouten, B.G.M. van Wachem, M.-O. Coppens, C.M. van den Bleek, Optimal placement of probes for dynamic pressure measurements in large-scale fluidized beds, Powder Technol. 139 (2004) 264–276.
[10] J. van der Schaaf, J.C. Schouten, F. Johnsson, C.M. van den Bleek, Non-intrusive determination of bubble and slug length scales in fluidized beds by decomposition of the power spectral density of pressure time series, Int. J. Multiphase Flow 28 (2002) 865–880.
[11] J.R. van Ommen, S. Sasic, J. van der Schaaf, S. Gheorghiu, F. Johnsson, M.-O. Coppens, Time-series analysis of pressure fluctuations in gas–solid fluidized beds – A review, Int. J. Multiphase Flow 37 (2011) 403–428.
[12] R. Chirone, F. Miccio, F. Scala, Mechanism and prediction of bed agglomeration during fluidized bed combustion of a biomass fuel: Effect of the reactor scale, Chem. Eng. J. 123 (2006) 71–80.
[13] J.R. van Ommen, J.C. Schouten, C.M. van den Bleek, An early-warning-method for detecting bed agglomeration in fluidized bed combustors, in: R.B. Reuther (Ed.), 15th International Conference on Fluidized Bed Combustion, ASME, New York, 1999, Paper No. FBC99–0150.
[14] M. Bartels, J. Nijenhuis, J. Lensselink, M. Siedlecki, W. de Jong, F. Kapteijn, J. R. van Ommen, Detecting and counteracting agglomeration in fluidized bed biomass combustion, Energy Fuels 23 (2009) 157–169.
[15] J.R. van Ommen, M.-O. Coppens, C. M. van den Bleek, J.C. Schouten, Early warning of agglomeration in fluidized beds by attractor comparison, AIChE J. 46 (2000) 2183–2197.
[16] J. Shabanian, F. Fotovat, J. Bouffard, J. Chaouki, Fluidization behavior in a gas-solid fluidized bed with thermally induced inter-particle forces, in: T.M. Knowlton (Ed.), 10th International Conference on Circulating Fluidized Beds and Fluidization Technology (CFB-10), Engineering Conferences International, New York, 2011.
[17] J. Bouffard, F. Bertrand, J. Chaouki, S. Giasson, Control of particle cohesion with a polymer coating and temperature adjustment, AIChE J. 57 (2012) 3685–3696.
[18] J. Shabanian, J. Chaouki, Pressure signals in a gas-solid fluidized bed with thermally induced inter-particle forces, in: J.A.M. Kuipers, R.F. Mudde, J.R. van Ommen, N.G. Deen (Eds.), 14th International Conference on Fluidization – From Fundamentals to Products, ECI Digital Archives, Noordwijkerhout, The Netherlands, 2013.
[19] J. Shabanian, J. Chaouki, Hydrodynamics of a gas-solid fluidized bed with thermally induced interparticle forces, Chem. Eng. J. (2014) submitted for publication.
[20] J. Shabanian, J. Chaouki, Local characterization of a gas-solid fluidized bed in the presence of thermally induced interparticle forces, Chem. Eng. Sci. (2014) submitted for publication.
[21] H.P. Cui, N. Mostoufi, J. Chaouki, Comparison of measurement technique of local particle concentration for gas–solid fluidization, in: M. Kwauk, J. Li, W.C. Yang (Eds.), Fluidization X, United Engineering Foundation, New York (2001) 779-786.
[22] M. Rüdisüli, T.J. Schildhauer, S.M.A. Biollaz, A. Wokaun, J. R. van Ommen, Comparison of bubble growth obtained from pressure fluctuation measurements to optical probing and literature correlations, Chem. Eng. Sci. 74 (2012) 266–275.
[23] H.T. Bi, J.R. Grace, Effect of measurement method on the velocities used to demarcate the onset of turbulent fluidization. Chem. Eng. J. 75 (1995) 261-271.
[24] H. Cui, N. Mostoufi, J. Chaouki, Characterization of dynamic gas-solid distribution in fluidized beds, Chem. Eng. J. 79 (2000) 133–143.
[25] H. Zhu, J. Zhu, New investigation in regime transition from bubbling to turbulent fluidization, Can. J. Chem. Eng. 86 (2008) 553–562.
[26] R. Clift, J.R. Grace, The mechanism of bubble break-up in fluidised beds, Chem. Eng. Sci. 27 (1972) 2309–2310.
[27] D. Moslemian, Study of solids motion, mixing, and heat transfer in gas fluidized beds, Illinois University, 1987.
[28] M. Stein, T.W. Martin, J.P.K. Seville, P.A. McNeil, D.J. Parker, Positron emission particle tracking: particle velocities in gas fluidized beds, mixers and other ppplications, in: J. Chaouki, F. Larachi, M.P. Dudukovic (Eds.), Non-invasive monitoring of multiphase flows, Elsevier, Amsterdam, The Netherlands, 1997, pp. 309–333.